Journal of Nanoparticle Research, Volume 23, Article number 97, 2021
DOI: 10.1007/s11051-021-05194-5

Titania containing natural clay doped with carbon nanotubes for enhanced natural photocatalytic discoloration of wastewater

A.A. Muleja[1]*, M.P. Mubiayi[1,2], F. Hassard[1,3], B.B. Mamba[1]*

[1] Institute for Nanotechnology and Water Sustainability (iNanoWS), College of Science, Engineering and Technology, University of South Africa, Florida Campus, Johannesburg 1710, South Africa [2] Mechanical and Industrial Engineering Department, College of Science, Engineering and Technology, University of South Africa, Florida Campus, Johannesburg 1710, South Africa [3] Cranfield University, College Way, Bedford, Bedfordshire, MK43 0AL, United Kingdom

*Corresponding authors: mulejaa@unisa.ac.za, mambabb@unisa.ac.za

Abstract

Water contamination with dyes is harmful to humans and the environment. This study investigated the photocatalytic activity of natural clay (GOL) mixed with carbon nanotubes (CNT) for removal of brilliant black (BB) in wastewater. The materials were characterized with FESEM-EDS, XRD, XRF, FTIR and UV-vis DRS. The natural clay contains 2.34 % TiO_2 which is 75 % more than most natural clays. SEM showed that CNT were well dispersed and mixed with clay. DRS spectra showed two absorption bands above 380 nm. CNT in GOL has decreased significantly the energy band gaps from 2.75 and 3.25 eV to 1.53 and 2.90 eV for GOL and 10 % CNT–GOL respectively. Photocatalytic activity was enhanced with degradation of BB increased from 66 % to 95 % with GOL and 10 % CNT–GOL respectively after 45 min of visible light irradiation. The improvement can be attributed to the synergy of the interface heterojunction of clay and CNT. The presence of CNT reduces the e^- and h^+ (e^- / h^+) pairs recombination, facilitates the production of reactive oxygen species responsible for the decay of dye. The addition of H_2O_2 to the experiment (2 mmoL) confirmed the role of holes and hydroxyl radicals. 85 % of BB carbon content was removed with 10 % CNT–GOL suggesting that mineralization occurred. After 45 min of visible light irradiation, the degradation kinetic studies followed a second-order reaction with a R^2 = 0.997. Therefore, natural clay–CNT nanocomposites can be applied to treat dyes containing wastewaters.

Key words: African clay; nanocomposites; mechanical mixing, heterojunction; photocatalysis; dyes.

Published by Springer. This is the Author Accepted Manuscript issued with: Creative Commons Attribution Non-Commercial License (CC:BY:NC 4.0).
The final published version (version of record) is available online at DOI:10.1007/s11051-021-05194-5. Please refer to any applicable publisher terms of use.

Introduction

The exploitation of industrial dyestuffs generates significant amounts of organics contamination in water through release of contaminated effluents. Azo compounds such as brilliant black (BB) are a complex class of dyes having a wide range of applications in textile, food, paint, plastics and cosmetics industries. The release of azo dyes into the environment is of great concern due to the colouration of natural waters, their toxicity, and the possibility of mutagenic and carcinogenic breakdown products (Oh *et al.,* 1997; Rafii *et al.,* 1997; Li *and* Bishop 2002; Todorova *et al.*, 2014; Brüschweiler *and* Merlot, 2017; Kausar *et al.,* 2018). Traditional methods for the disposal of dyes in wastewaters (e.g. filtration, coagulation, ion-exchange, granular activated carbon and ion exchange resins) are costly and generate hazardous secondary pollution problems (Molinari *et al.,* 2017). Traditional advanced oxidation processes (AOPs) offer enhanced dye destruction and low by-product and secondary pollution problems compared to traditional dye treatments (Al-Kdasi *et al.,* 2004). Natural methods for dye decolourisation such as clays adsorbents have gained attention as they are inexpensive, can be sourced local to pollution source and empower community led treatment initiatives (Kausar *et al.,* 2018). However, dye treatment using natural clays can result in secondary pollution through desorption into water courses. Thus, there is a need for the development of new technologies that can remove these hazardous compounds in water and wastewater (Al-Kdasi *et al.,* 2004; Molinari *et al.,* 2017). Therefore, the synergy of adsorption, degradation and mineralization of the dyes by enhanced materials represent a strategy to treat dyes at source.

Photocatalytic oxidation of organic compounds present in wastewater using photochemical reaction occurring on a semiconductor catalytic solid surface activated by solar light irradiation has shown promise for dye treatment (Saleh *and* Gupta, 2012). Chen *et al.* (2004) found that adsorption is significantly effective to enhance the rate of photodegradation of dyes under visible light irradiation. Herrmann (1999) reported that photocatalysis relies on the aptitude of the photocatalyst to simultaneously adsorb both reactants and to absorb efficient photons and the migration of light-induced electron holes. Titania (TiO_2) is an effective photocatalyst as it has a large band gap energy, physico-chemical stability, non-toxic, cost-effectiveness and is insoluble. However, the efficiency of TiO_2 is reduced due to e^- / h^+ pair recombination. Adding a co-

adsorbent is a good strategy for increasing the photocatalytic efficiency of TiO_2 (Saleh *and* Gupta, 2012). It is therefore expected that using natural clays would combine the advantages (adsorption and photoresponse) of each compound of the reported materials (Asif *et al.* 2015; Hamza *et al.,* 2018; Martínez-Costa *et al.,* 2018) to enhance the removal of dyes pollutants from dye containing wastewaters. Natural clays could be utilized as photocatalysts due to the high photochemical activity in the degradation of contaminants, high chemical stability, accessibility and low cost (Martínez-Costa *et al.,* 2018). For instance, da Silva Lopes *et al.* (2019) have recently indicated that the mixture of the TiO_2 dispersion with purified natural kaolinite resulted in the formation of nanocomposites with good catalytic properties.

CNT can be produced in a semi-conducting, semi-metallic or metallic form (Ebbesen *et al.,* 1996; Collins *and* Avouris, 2000). We hypothesised that CNT could significantly enhance GOL photocatalytic performance as CNT acts as a semiconductor reducing e^- / h^+ pairs recombination. CNT is thought to improve photocatalysis of complex organic molecules through positive h^+ formation in the valence band and e^- occupied the conduction band which generates radicals. If the e^- / h^+ pairs recombine the photocatalytic efficiency is reduced. The combination of CNT with other materials leads to a new generation of donor-acceptor nanocomposites, which, upon illumination, give a fast charge separation and a slow charge recombination. CNT should be even more suitable for achieving charge transfer and charge transport (Guldi *et al.,* 2005). Indeed, some studies (Saleh *and* Gupta, 2012; Yin *et al.,* 2016) have proven that the e^- accepting and e^- transport properties of CNT provide a convenient way to direct the flow of photogenerated charge carriers. The excited e^- in the conduction band of TiO_2 may migrate into CNT, of which have a special structure and the ability for e^- transport. Thus, the possibility of the recombination of e^- / h^+ pairs decreases more radicals are in the system, resulting in faster degradation of the dyes (Yu *et al.,* 2005). Natural clays rarely contain sufficient TiO_2 considered > 1 wt. % for enhanced photocatalysis (Hamza *et al.,* 2018; Martínez-Costa *et al.,* 2018). In this study, natural clay from Golf–Katanga region (GOL clay) in the DR Congo was used due to a TiO_2 content > 1 %. The method to mechanically mix different materials such as zeolite and TiO_2 (Yamaguchi *et al.* 2009) and TiO_2 with MgAl-LDH (Paredes *et al.* 2011) to form composites with high performance photocatalytic properties has been reported previously. To the best of our knowledge, GOL and CNT have not been used previously for the removal of dyes from water.

Therefore, the aim of this study is to i) understand the impact of CNT dose (5 and 10 wt. %) on the photocatalytic performance and ii) investigate whether the azo dye compound could be mineralised using natural solar radiation. The photocatalytic activity was achieved through controlled degradation experiments using these materials under visible light irradiation. The superior adsorption ability of the photocatalytic materials (GOL mixed CNT) was used to the advantage of photodegradation to ensure enhanced capture, degradation and mineralization of dyes molecules (Yu *et al*., 2005; Asif *et al.,* 2015; Hamza *et al.,* 2018; Martínez-Costa *et al.,* 2018). The principal focus of this investigation was solely on the photocatalytic activity of the mixed nanocomposites.

Experimental methods

Materials

The natural clays used in this study originated from Golf coded as GOL, Katanga province in the Democratic Republic of the Congo (DRC). Multi-walled carbon nanotubes (CNT) were produced from ferrocene (2.0 g) dissolved in toluene (50.0 mL) through a nebulised spray pyrolysis (NSP) technique reported in the literature (Muleja *et al, 2012*). A modified method to mechanically mix two materials into photocatalysts was followed (Yamaguchi *et al*. 2009). Briefly, the GOL clay was pulverized using a Siebtechnik Puck Mill Ring Mill Pulverizer and mechanically mixed with CNT to make 3 different ratios. The ratios represented are 100/0 (% w/w) for 100 % GOL–0 % CNT; 95/5 (% w/w) for 95 % GOL–5 % CNT and 90/10 (% w/w) for 90 % GOL–10 % CNT. The mixture was then thoroughly ground resulting in homogeneous products. The brilliant black (BB: dye content 60 %) and the hydrogen peroxide solution (H_2O_2: > 30 %) were purchased from Sigma-Aldrich. Milli-Q ultrapure water was used throughout the experiments unless otherwise stated.

Characterization of GOL, 5 % CNT–GOL and 10 % CNT–GOL

The X-ray Fluorescence (XRF) analysis using a Rigaku, ZSX Primus II was performed on the GOL sample to obtain the chemical composition. Pallets of GOL sample were made and dry in

an oven for 24 hours to remove the moisture. Bulk chemical compositions (phase identification) of the GOL and the admixtures were recorded on a XRD (Ultima IV X-ray diffractometer, Rigaku) equipped with a graphite-monochromated Cu Kα radiation source (40 kV, 30 mA) with 2θ range of 10° to 90° , step size of 0.01 and scan speed of 0.5° min^{-1}. A JEOL JSM-7800F Field Emission Scanning Electron Microscope (FESEM) instrument coupled with Thermo Scientific Ultradry energy-dispersive X-ray spectroscopy (EDS) detector was used for the surface morphology analysis and to identify chemical elements and their distribution on the samples. The Fourier-transform infrared spectroscopy (FTIR) spectra of the samples were recorded by using a Perkin–Elmer Frontier FTIR spectrometer. The samples were scanned with 16 background accumulations in the range of 450–4000 cm^{-1} at the spectral resolution of 4 cm^{-1} by using the KBr pellet method. A PerkinElmer lambda 1050 UV/VIS/NIR Spectrometer was combined with a reference material comprised of barium sulfate. The diffuse reflection spectroscopy (DRS) were acquired in the range of 200 to 800 nm. Absorption spectra were transformed according to the Kubelka−Munk relationship to understand the absorption characteristics of our materials and calculate the optical band gaps. The total organic content (TOC) measurements were carried out using a TOC torch (Teledyne Tekmar, USA) instrument. Standard solutions of 0 ppm, 5 ppm, 10 ppm, 25 ppm and 50 ppm carbon were prepared using potassium hydrogen phthalate (KHP) and DI water. Calibration standards were measured prior to sample analysis for instrument calibration.

Photocatalytic degradation evaluation

The photocatalytic degradation experiments were carried in a similar manner as previously reported (Muleja *and* Mamba 2018). In brief, degradation experiments were undertaken in a solar simulator (HAL–320 Asahi Spectra, Japan) which produced the required spectral irradiance and dose. A 300 W Compact Xenon light with apparent power 500 VA was used as the light source. The solar simulator radiation spectrum output wavelength ranges were set from 350 to 1100 nm, and an air mass filter (1.5 Global filter) was placed in front of the lamp to eliminate most of the UV radiation. The intensity distance which was the distance from the collimator lens to the sample surface was set at 37 mm. It created an effective radiated area of 50 mm^2 and an irradiance of approximately 100 mW cm^{-2}. Typically, all the materials (25 mg) were mixed with

BB solution (5ppm, 50 mL). The mixture was stirred in the dark for 60 min to establish the adsorption-desorption equilibrium. A sample was drawn from the solution using a syringe unit fitted with 0.45 µm pore size hydrophilic PVDF membrane. The first sample drawn after adsorption-desorption equilibrium was considered as the initial concentration (C_i). The solar simulator was prewarmed (30 min) for stable irradiance output and samples (mixed solution of photocatalysts and BB) were subsequently irradiated in a 100 mL quartz beaker. Samples were drawn from the solution at 15 min intervals, filtered and analysed using a UV-vis spectrometer (Lambda 650S, Perkin Elmer, USA). The experiments were undertaken for 60 min and were stirred using a magnetic bar. The UV-vis photometric measurements of standards and samples were done at maximum absorbance 571.3 nm (BB wavelength: 567–573 nm) to obtain the concentration of BB after the elapsed time interval (C_f). Experimental data from the effect hydrogen peroxide solution on the photocatalytic degradation of BB were collected in the similar manner, except that H_2O_2 was added to the mixed solution (BB and all three materials) and at various concentrations namely 2 mmoL, 4 mmoL and 6 mmoL. A calibration curve was obtained from the standards and the percentage photocatalytic removal of BB dye was calculated after (1):

$$\%Degradation = \frac{C_i - C_f}{C_f} \times 100 \quad (1)$$

Results and discussion

Morphology analysis of CNT, GOL and 10 % CNT–GOL

The micrographs of three materials namely the CNT, GOL and 10% CNT-GOL are shown in Figure 1 (a-d). CNT morphology (Figure 1 a) were significantly different compared to the clay (Figure 1 b). However, when the two were mixed, the surface morphology of these materials shows the presence of well-dispersed clay consisting of particles of different sizes forming blocks of variable thickness in Figure 1 (c) at the micrometre resolution. When the resolution was lowered in the nanometre, nanotubes are clearly visible on the nanocomposite 10 % CNT–GOL as shown in Figure 1 (d). High magnification image of FESEM depicted in Figure 1 (b) showed layers on the natural clay (raw GOL). The presence of these layers could be crucial for

the removal of BB dyes, through provision of effective photocatalytic reaction area. The raw GOL sample also showed pores structures which represent an advantage for adsorption and subsequently photocatalytic activity (Figure 1 b). The high definition SEM pictures of the mixed materials (Figures 1 (c) and (d)) are composed of carbon nanotubes well mixed with clays cumulative form of aggregated different-shaped particles. The incorporation of CNT appeared on the surface of clay as previously reported (Gournis *et al.*, (2002) and Terzopoulou *et al.*, 2016).

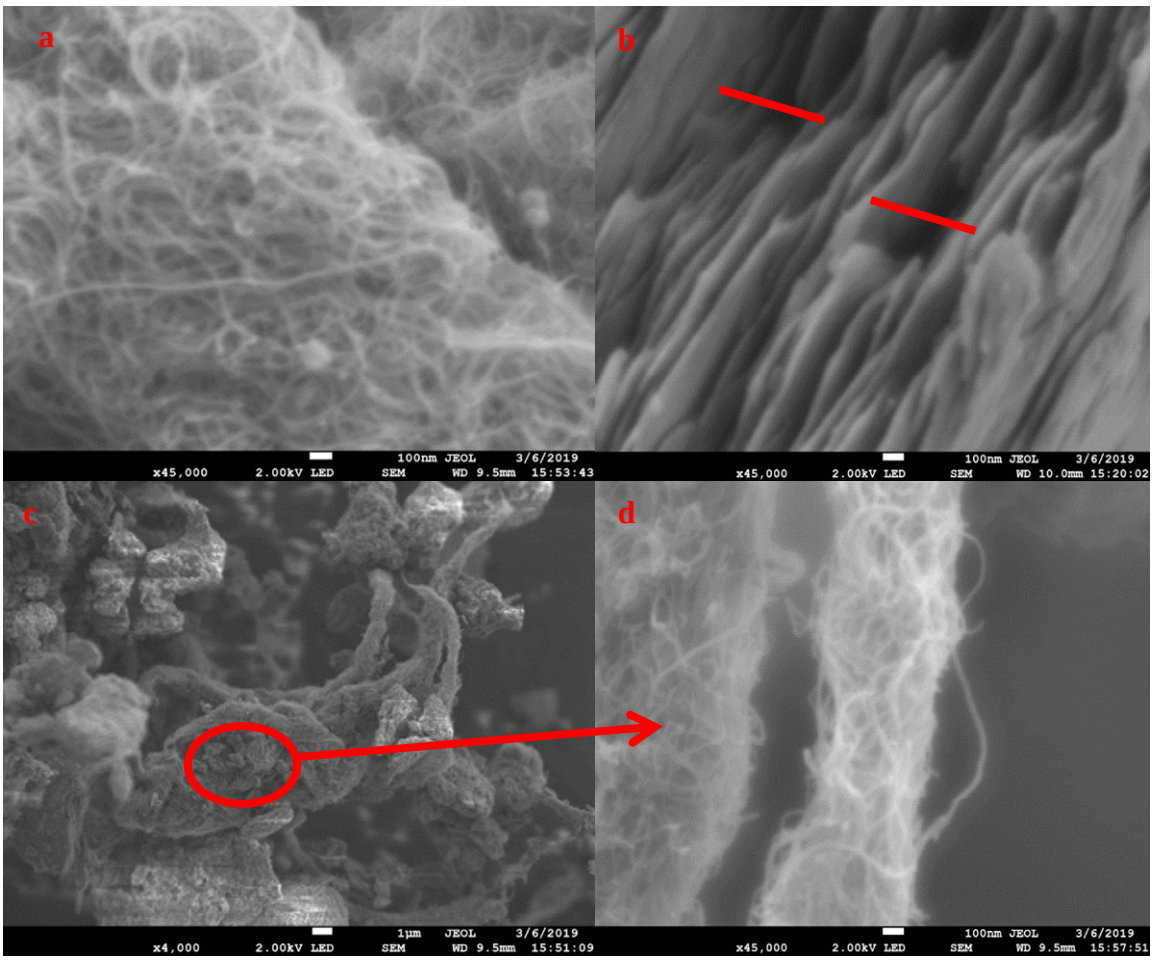


Figure 1. FESEM surface morphology images of (a) CNT; (b) GOL clay; (c) low magnification 10 % CNT–GOL and (d) high magnification of 10 % CNT–GOL. Red lines represent pores and layers.

Characterization of 10 % CNT–GOL elemental composition

Elemental mapping analysis of GOL clay and GOL clay mixed with CNT was measured. The elemental distribution of 10% CNT–GOL clay show the presence of elements such as oxygen (O), silicon (Si), aluminium (Al), iron (Fe), potassium (K) and titanium (Ti) (Figure 2 a) which is expected and in agreement with previous reports on natural clays (Yu *et al.,* 2005; Martínez-Costa, *et al.,* 2018). The energy-dispersive x-ray spectroscopy (EDS) spectrum of 10% CNT–GOL clay sample confirming the presence of each element found by the mapping analysis (Figure 2 b). The elemental distribution on the maps indicates that the intensity of elements O, Si, Al, Fe, K and Ti follow a decreasing order, respectively. The results reveal a high concentration of Si and Al whilst Fe, K and Ti are less abundant. Further analysis of the surface topography showed that GOL are dominated by oxygen and the following mineral phases including SiO_2, Al_2O_3, TiO_2, Fe_2O_3 which offer varying levels of photocatalytic activity (Martínez-Costa *et al.*, 2018).

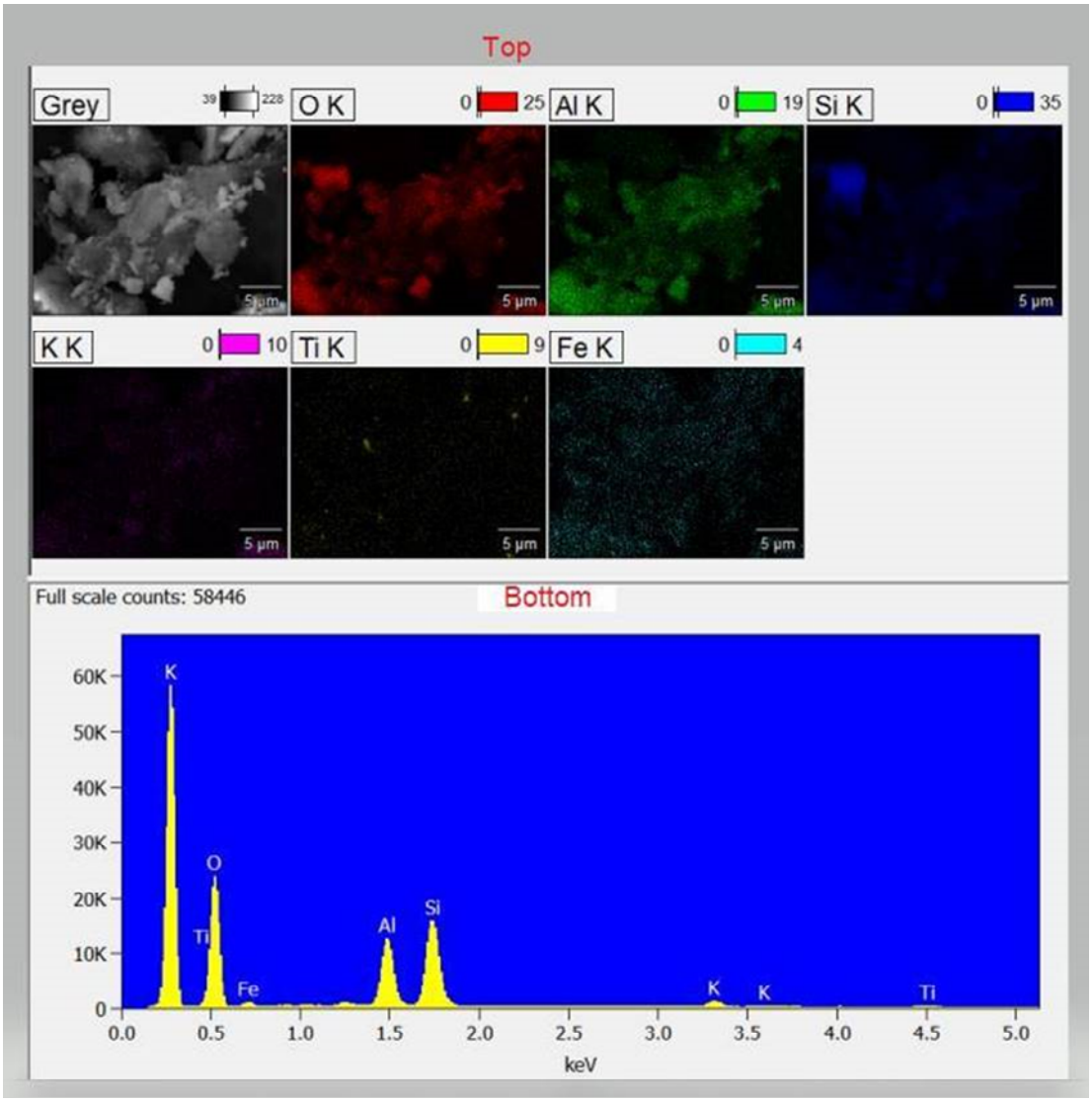


Figure 2. Top) Elemental mapping distribution of 10% CNT–GOL clay sample; bottom) energy-dispersive X-ray spectroscopy spectrum of 10% CNT–GOL clay

Chemical composition determination of GOL clay

CNT–GOL clay sample was not analysed because X-ray fluorescence (XRF) is limited to detect carbon content. The chemical composition of GOL clay was determined with XRF spectrometer (Table 1) and have a similar profile to other natural clays (Martínez-Costa *et al.,* 2018). However, the concentration of TiO_2 is higher (2.34%) than for the other natural clays, 0 % (Hamza *et al.*, 2018) and 0.58 % (Martínez-Costa *et al.,* 2018), which is an advantage of the

GOL clay because TiO_2 is often desired for photocatalytic activity. The high contents of silica, alumina, hematite and titania are of great importance for the application of these materials in photocatalysis. Additionally, the clay and its composition namely silica, alumina, hematite and titania have been used significantly in the adoption of contaminants from aqueous solution separately and or combined with other compounds (Kausar *et al.*, 2018). Moreover, Hermann (1999) has reported that adsorption is a crucial stage of the photocatalysis process. The XRF results shown in Table 1 display the presence of chemical elements namely O, Si, Al, Fe, K and Ti which is consistent with the EDS analysis in Figure 2 (b).

Table 1 – Mass percentage of chemical elements in GOL.

Component	**Mass %**
SiO_2	64.04
Al_2O_3	23.02
Fe_2O_3	5.98
K_2O	2.37
TiO_2	2.34
MgO	0.87
CaO	0.36
P_2O_5	0.23

Chemical phases determination and functional groups identification of GOL, 5% CNT–GOL and 10 % CNT–GOL

The X-ray diffraction (XRD) patterns of (black colour) GOL clay, (red colour) 5% CNT–GOL clay and (green colour) 10% CNT–GOL clay samples are shown in Figure 3 (A). The XRD technique was instrumental to determine the bulk structure and composition of materials with crystalline structure. The analysis revealed that GOL are constituted by mineral phases including quartz (SiO_2) (ICDD (PDF2010): 01-082-1572), cristobalite (SiO_2), karrooite ($MgTi_2O_5$) (ICDD (PDF2010): 01-075-9297), perovskite ($Ca(TiO_3$) (ICDD (PDF2010): 01-088-0790), mullite ($Al_5SiO_{9.5}$) (ICDD (PDF2010): 01-088-2049). The presence of silicon is evidence of SiO_2 as shown at peaks 2-theta ranging from 21 º Cristobalite (1,1,3), silicon dioxide (1,1,1), Cristobalite

(1,0,1) and 28 º silicon dioxide (3,0,0), Karrooite, (6,3,0),Mullite, (16,2,2) and, Perovskite (2,3,1). The shift in peaks was attributed to different phases of SiO_2 and probably the blending with CNT as well. Similar peaks at 2 θ = 26.8 º are Mullite, (11,1,3) and Karrooite, (1,1,1) and 42.6 º corresponding to graphite in a clay-multiwalled CNT sample have been reported previously (Zhu *et al.,* 2004; Oh *et al.*, 2010). The peaks corresponding to TiO_2 from karrooite (1,1,1), perovskite (1,3,1), mullite (10,2,0) and Perovskite (1,2,0) are identified at 2 θ = 36.81, 45.77, 55.14 and 62.41, 77.90 º while quartz can also be found at peak 68 º. SiO_2 and Al_2O_3 are the main components of these samples and this is confirmed by bulk structures available bearing these phases including aluminium oxide silicate. Masheane *et al.* (2018) confirmed that silica and alumina as the major constituents of the clay. Peaks identified at 2 θ of 24.28 °, 42.70 °, 50.38 °, 64.29 °, 81.42 ° are assigned to hematite phases. Furthermore, other elements (including calcium and potassium) identified by EDS and XRF are in the forms of diopside and potassian minerals of the clay. The XRF, XRD and EDS results revealed that the clay contains mainly SiO_2, Al_2O_3, Fe_2O_3 and TiO_2 which was successfully used as photocatalyst for the degradation of the methabenzthiazuron herbicide in water (Khennaoui, *et al.*, 2020).

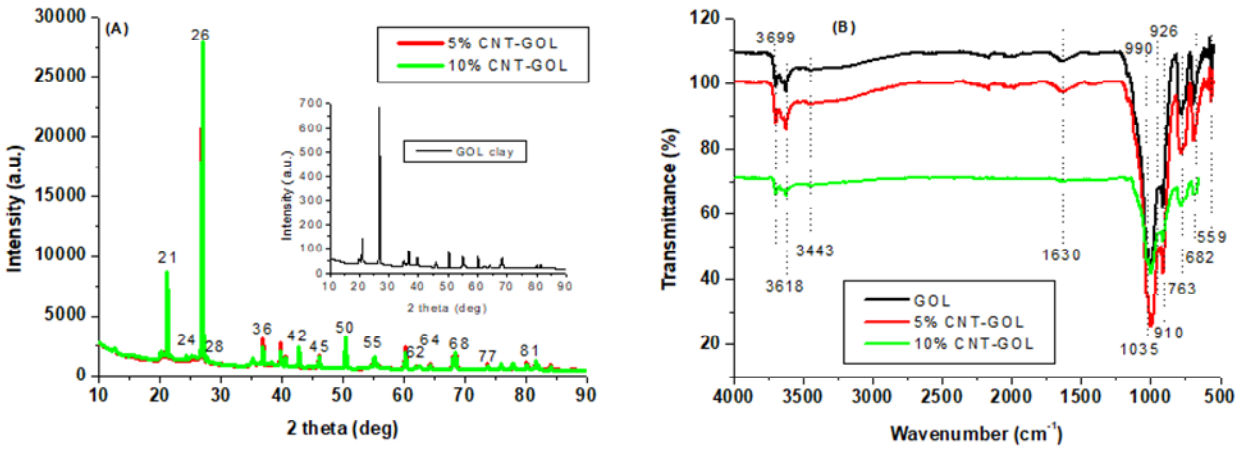


Figure 3. (A) XRD patterns and chemical phase peaks and (B) FTIR spectra of GOL clay; 5 % CNT–GOL and 10 % CNT–GOL samples.

The Fourier-transform infrared spectroscopy (FTIR) spectra of GOL clay, 5 % CNT–GOL clay and 10 % CNT–GOL clay samples are shown in Figure 3 (B). The spectra show two peaks at

3698 cm^{-1} and 3618 cm^{-1} band due to stretching vibration hydroxyls. Minor bands at 3443 cm^{-1} for GOL clay blended with CNT were due to internal hydroxyls linked to the aluminium (Chargui *et al.*, 2018). The absorption band presented at 1630 cm^{-1} can be attributed to the binding vibration of water molecules (which can be found between 1600 to 1650 cm^{-1}) (Boukhemkhem *and* Rida, 2017; Hadjltaief *et al.*, 2019) and or deformation of hydroxyl groups (O–H) (Leow *et al.*, 2016). The sharper peak between 990 and 1035 cm^{-1} for the samples corresponds to silicon-oxygen bonds present in the clays (Terzopoulou *et al.*, 2016; da Silva Lopes *et al.*, 2019). The peak around 763 cm^{-1} is believed to be due to Ti-O-Ti bonds while the absorption of Ti-O-Si is found around 926 cm^{-1} (Zeitler *and* Brown, 1957). The presence of the band at 910 cm^{-1} is assigned to the Al–OH units linked to bulk structures of the clay samples (Boukhemkhem *and* Rida, 2017; Chargui *et al.*, 2018) and to the OH bending for clay admixed with CNT (Terzopoulou *et al.*, 2016). The bands at 682 and 559 cm^{-1} correspond to the vibrations of Si–O–Al groups (Boukhemkhem *and* Rida, 2017; da Silva Lopes *et al.*, 2019). The functional groups identified agree with the chemical elements present as shown by elemental mapping and EDS spectrum in Figure 2.

Optical analysis of GOL; 5 % CNT–GOL and 10 % CNT–GOL

The raw clay and clay with CNT were analysed for their photoresponse ability in order to confirm suitability as photocatalysts. The optical technique measurements were undertaken on GOL clay, 5% CNT–GOL, 10% CNT–GOL and on CNT (Figure 4). Figure 4 (a), (b) and (c) shows Kubelka–Munk function plots that were derived from the DRS as previously reported (Muleja *and* Mamba 2018). The diffuse reflectance UV–vis spectrum (DRS) of the CNT reveals a shift in the far and near ultraviolet between 200 and 300 nm respectively, and no other absorption was observed thereafter which agrees with previous work (Cheng *et al.*, 2011). However, Khennaoui *et al*. (2020) have reported that Algerian natural clay showed an intense UV-vis absorption band situated at 201 nm and four weak bands situated at 243, 248, 366 and 430 nm. It was thought that balance between SiO_2 and TiO_2 could alter the photocatalytic activity of the mechanical mixed clay in this study. The investigation of these materials (GOL clay, 5 % CNT–GOL, 10 % CNT–GOL) showed reflectance on the violet light for example at 320 nm and another reflectance in the blue light ranging from 450 nm to 495 nm. This provided

circumstantial evidence of the photocatalytic activity in both the UV and the visible lights, suggesting solar radiation may function as a suitable energy source. Two bands edge were observed for the GOL clay, 5 % CNT–GOL and 10 % CNT–GOL. The two absorption edges emanate from bulk structures and different phases of minerals revealed by XRF and XRD in Table 1 and Figure 3 (A), respectively. For example, TiO_2 is known to possess two phases namely rutile and anatase which are responsible for two absorption edges in the composite sample (Nazarkovsky *et al.,* 2014). Figure 4 (d) implies that the materials combine the features of GOL clay (SiO_2, Al_2O_3, TiO_2, Fe_2O_3) and CNT resulting into new properties which could modify the process of the e^- / h^+ pair formation (Saleh *and* Gupta, 2012). It is suggested that CNT improves the function and formation of the e^- / h^+ pair improving performance and stability of these materials for solar photodegradation of dyes in aqueous solutions.

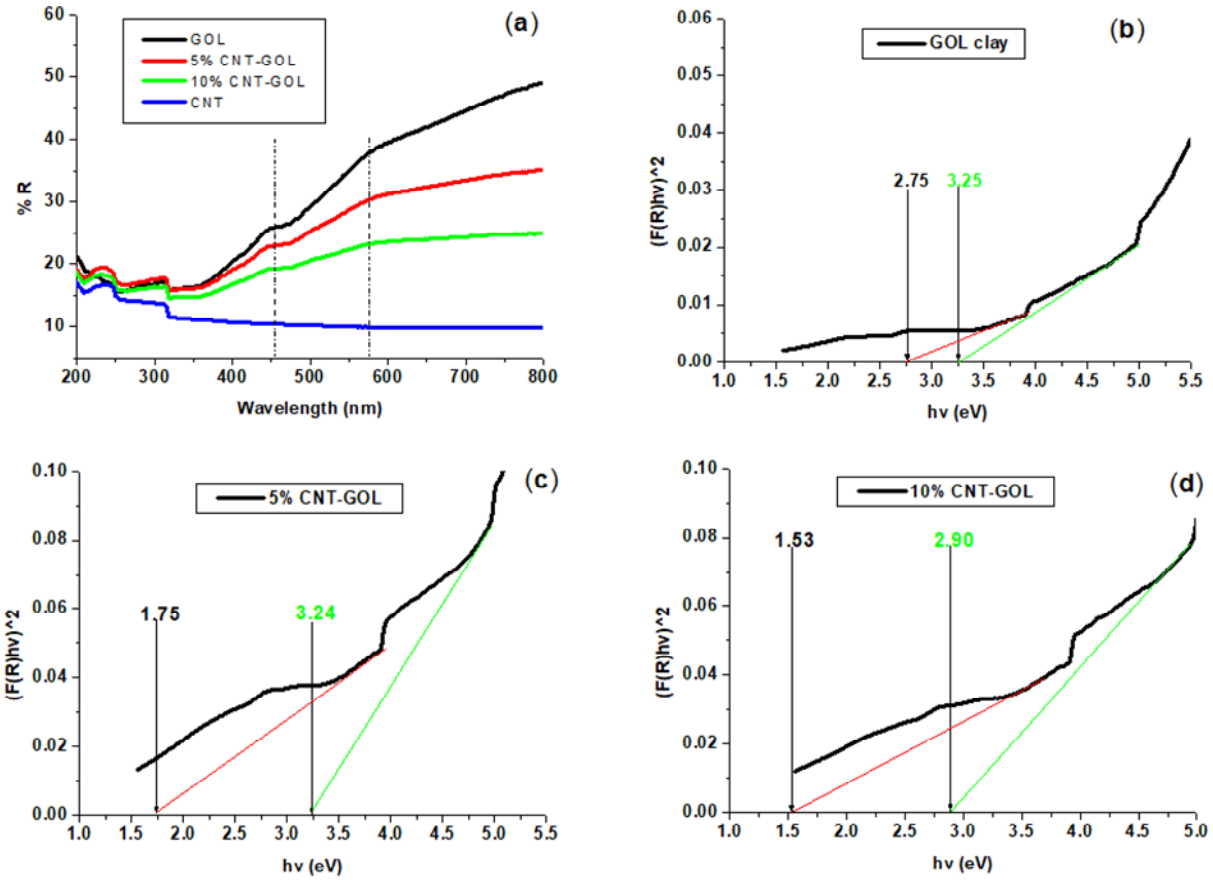


Figure 4. (a) DRS of CNT, GOL clay, 5 % CNT–GOL and 10 % CNT–GOL showing absorptions above 380 nm and the Kubelka-Munk plots for (b) GOL clay, (c) 5 % CNT–GOL and (d) 10 % CNT–GOL depicting the energy band gaps values.

The energy band for these materials was measured from the Kubelka–Munk function and the Tauc's relation of a curve $(F(R)hv)^2$ *vs hv*. Where *hv* is the photon energy and *F(R)* the reflectance factor that was transformed according to the Kubelka–Munk model from the reflectance R. The results (Figure 4 (a), (b) and (c)) show two energy band values for each material most likely due to different phases which characterize both pure GOL clay and mixed CNT–GOL samples. For GOL sample, the energy band gaps values are 2.75 eV and 3.25 eV within the range of previously reported values (Horwath *and* Liang, 2011). Horwath *and* Liang (2011) reported that the energy band gap values of clays range from 1.5 eV to 6.5 eV. They also observed that the band gap energies vary depending on the chemical composition and overall

atom % of the clay. In this study, the energy band gaps values are 1.75 and 3.24 eV, and 1.53 and 2.90 eV for 5% CNT–GOL and 10% CNT–GOL, respectively. The lowering of the energy band gap for these materials without considering the effect of CNT could be due to the presence of hematite whose energy band gap is reported to be 1.9–2.3 eV (Matsumoto, 1996; Guo, 2007). Furthermore, the energy band gap of TiO_2 is generally accepted to be 3.20 eV (Djouadi *et al.*, 2018) hence contributing to the values obtained for the present materials. However, the decrease of the energy band gap for the CNT–GOL clay samples was attributed to CNT. This is because of the diversity in energy band gap in CNT which ranged from zero (metal-like) to as high as that of silicon because of the difference in the size and the structure (Collins *and* Avouris, 2000; Wei *et al.,* 2013). Wei *et al.* (2013) have reported even smaller values of the energy band gap (0.97, 1.09, and 1.02 eV) for pure and treated carbon nanotubes. The evidence shows that the introduction of CNT in the GOL clay has decreased the energy band gap from 3.25 eV to 1.53 eV. Hence, it is confirmed that the interaction between CNT and GOL clay would enhance the photocatalytic properties through formation of heterojunction.

Photocatalytic activity

Removal of BB dyes: effect of irradiation time and addition of H_2O_2

The removal of BB dyes from aqueous solution through photocatalytic degradation was measured with UV-vis spectroscopy. Figure 5 (a) shows that the removal of BB dyes increased for all three materials and decreased after 45 min of irradiation time. The results reveal that the removal of BB dyes improved gradually with the addition of 5 % CNT and 10 % CNT to GOL clay with the highest percentage achieved with 10 % CNT addition. The positive link between BB removal and CNT addition indicated that CNT addition plays an important role stabilising this oxidation process. At 45 min of irradiation time, the percentage of degradation was 65.76 %, 79.44 % and 94.71 % for GOL clay, 5 % CNT–GOL and 10 % CNT–GOL, respectively. In this study clay nanocomposites have demonstrated photoresponse as illustrated in Figures 4 and 5. The removal of BB dyes could be attributed to the ability of clay and CNT to adsorb dyes on the photocatalysts. Both clay and CNT can behave as semiconductors. It is thought that the BB dyes are transferred through diffusion onto the semiconductors. The adsorption of BB dyes to the

photocatalysts surface and excitation of the photocatalysts generates oxidizing radicals which unselectively degrade the macromolecule dyes. CNT acts as an efficient adsorption trap of the dye leading to rapid photocatalytic degradation (Saleh *and* Gupta, 2012). Although adsorption is basic in photocatalysis, the current investigation emphasises on the photocatalytic features of the combined clay and CNT samples.

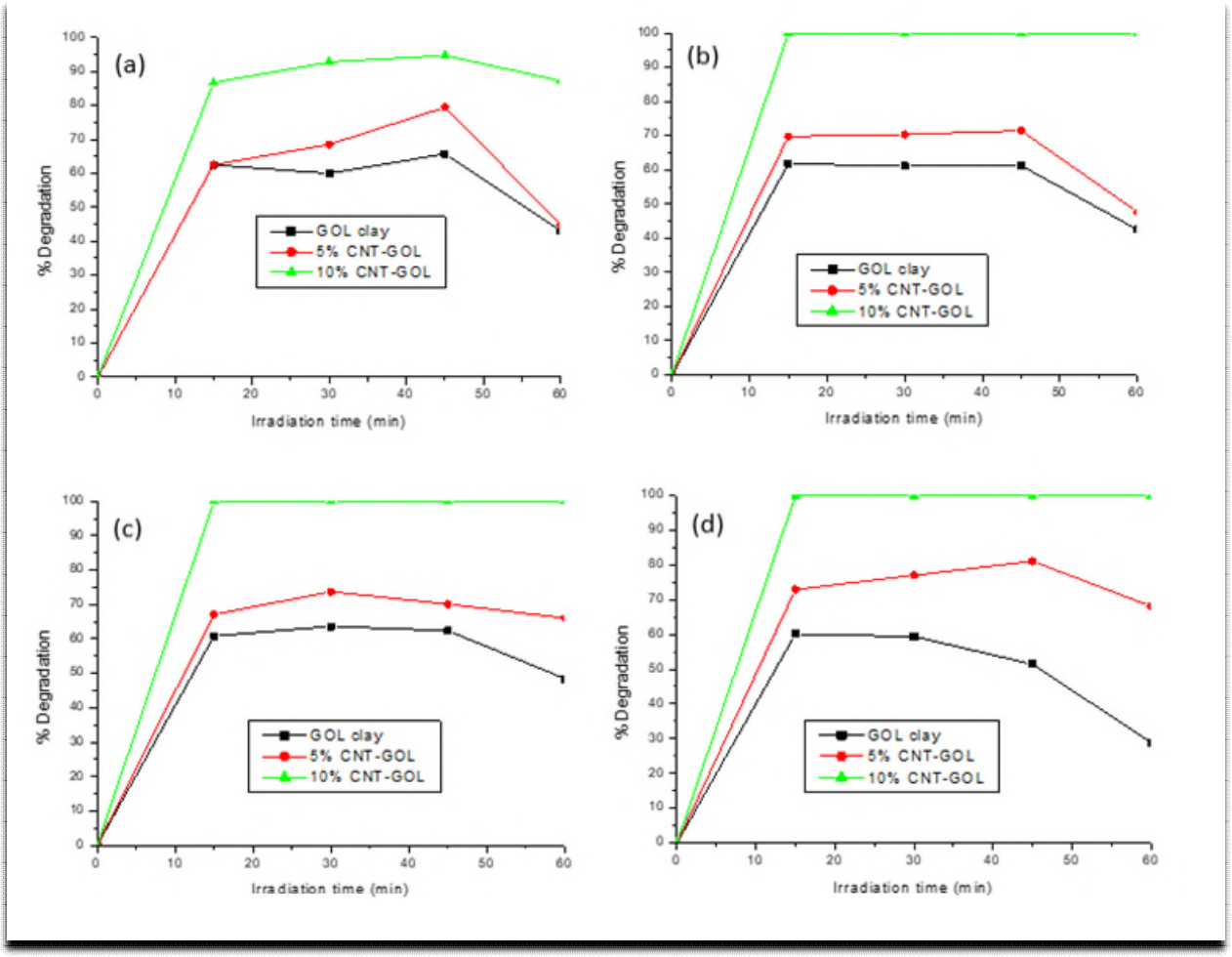


Figure 5 (a). Photocatalytic activity of GOL clay, 5% CNT–GOL and 10% CNT–GOL in the degradation of BB dyes under visible light irradiation; for (b) 2 mmol; (c) 4 mmol and (d) 6 mmol of H_2O_2 was added respectively.

Further experiments were carried out in a similar way but the only difference being the addition of hydrogen peroxide (H_2O_2) to the mixed slurry of photocatalysts containing the BB dye

aqueous solution and the results are displayed in Figure 5 (b), (c) and (d). When 2 mmol, 4 mmol and 6 mmol of H_2O_2 were added to the suspensions, the photocatalytic activity of 10 % CNT–GOL increased up to 100 % degradation of BB dye in 15 min. At the same time the photodegradation of BB with GOL clay and 5 % CNT–GOL clay was 61.77 % and 69.75 % for 2 mmol (H_2O_2); 60.85 % and 67.08 % (4 mmol (H_2O_2), and 60.07 % and 72.90 % for 6 mmol (H_2O_2), respectively. Overall, these findings indicate that the amount of CNT added to the GOL clay is as much important as H_2O_2 to a certain extend. 10% CNT–GOL clay had the highest photocatalytic activity, reaching 86.68 % and 100 % degradation of BB dyes in 15 min without H_2O_2 and with H_2O_2, respectively (Figure 5 a, b). On the other hand, 62.49 % and 86.68 % of dyes were removed with GOL clay and 10 % CNT–GOL clay, respectively within the same irradiation time. The photodegradation was 24.19 % higher when CNT was added to the clay without the addition of H_2O_2 and 13.32 % with H_2O_2. Improved BB dyes photodegradation was achieved with the combination GOL and CNT, addition of an additional source of radicals led to reduced degradation rates, possibly due to radical scavenging.

These data show that when 10 % of CNT is added to the natural GOL clay, 94.71 % of BB dye pollutant are removed from the aqueous solution. The results also show that only small amount of H_2O_2 is enough to reach the highest value 100 % of BB dye removed within 15 min. Therefore, the findings imply: i) using the GOL clay acts as an interface and provider of semiconductors (structural phases (XRD) and chemical compositions (XRF)); ii) mixing with CNT (an electron giver and acceptor) coupled with 2 mmol of H_2O_2 (producer of oxidising species (hydroxyl and superoxide radicals)) could have contributed to the photoresponse of the utilised materials as confirmed by DRS results. Other characterisation techniques include FESEM, Maps-EDS and FTIR used revealed functional groups linked to titania, silica, alumina and hematite and a good distribution of each chemical element associated thereto in samples confirming their presence and possibility to react during the photocatalysis of BB dye. More details about possible phenomena interactions that are susceptible to occur are entailed in the mechanism section of this paper.

Figures 6 (a) to (d) show the photocatalytic activity of the raw and admixtures materials on the concentrations decay of BB dye as a function of irradiation time. The results confirm the trends

observed in Figures 4 and 5. The data indicate the disappearance of BB dye with irradiation time until 45 min for Figure 6 (a) whereas for Figure 6 (b), (c) and (d) different tendencies are obtained. The results obtained with 10% CNT–GOL suggest that there is an improvement in the performance which can be attributed to the synergy of the various components. These include structural chemical composition of GOL clay, CNT and the addition of H_2O_2. Photocatalytic reaction accounts for the electronic structure of the photocatalyst and there are two critical factors that influence photocatalysis namely light absorption by the material and migration of light-induced electron holes (Asif *et al.*, 2015). The combination might contribute to the collective features of a good photoresponse from the photocatalysts based on the ability to generating oxidising species such as hydroxyl and superoxide radicals, charge separation and transportation.

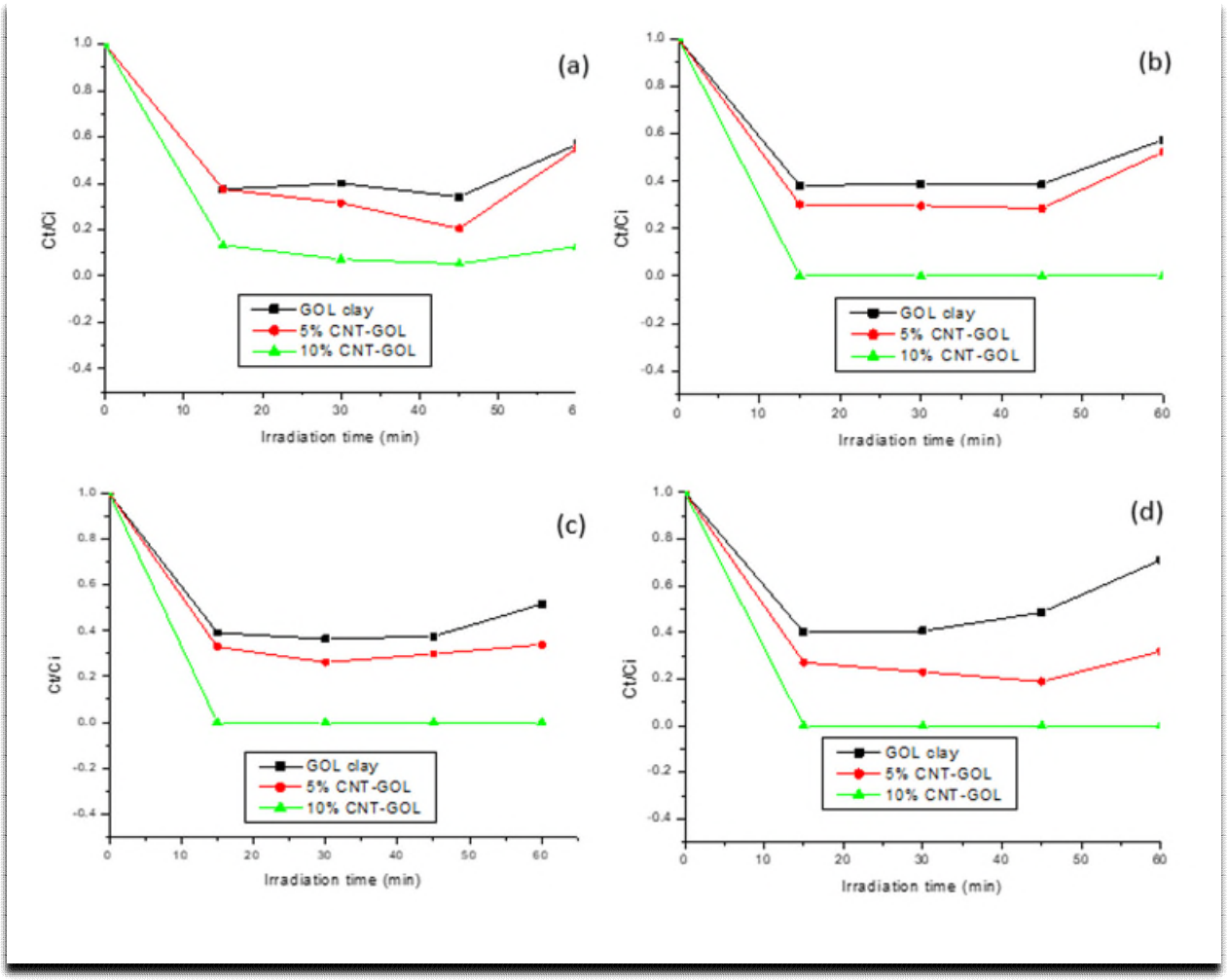


Figure 6. (a) Mineralisation of BB dyes using GOL clay, 5% CNT–GOL and 10% CNT–GOL as photocatalysts under the visible light irradiation time; and for (b) 2 mmol, (c) 4 mmol and (d) 6 mmol of H_2O_2 was added, respectively.

Photodegradation could be detailed as a combination of improved adsorption of dye molecules onto the catalyst surface, charge separation and transportation, visible light absorption, generation of sufficient amounts of the oxidising species of the photocatalyst (Mamba *et al.* 2014). The data presented in Figures 5 and 6 can be grouped in three scenarios: *i*) Some of the dyes adsorbed during the initial step of the experiment (60 min run in the dark: not shown) might have not been completely decomposed with clay and clay mixed with 5% CNT. The absorbed light might not have been enough due to the small amount of CNT in the nanocomposite. So, some of the adsorbed dye molecules might have been released (after 45 min) into the solution during the photocatalytic experiment. To mitigate such shortfall, more time and or enough CNT might be required to facilitate generation of enough oxidizing species and the charge separation and transportation for complete decay of the dyes. *ii*) When hydrogen peroxide was added to the mixture particularly for 10 % GOL–Clay, enough reactive oxidizing species were formed in the aqueous solution resulting in the complete decomposition of dyes. In this case, the adsorbed dyes during the 60 min dark experiment including enough light absorbed during the light experiment could have enhanced the synergy of GOL–CNT mixture prompting total discoloration in 15 min. 10% CNT–GOL reveals most of the features of reported good photocatalysts (Saleh *and* Gupta 2012) which could explain the fast initial (15 min) decrease of dye concentration observed. The recombination kinetics of charge carriers might have been reduced and/or eliminated by the synergy of clay composition and CNT hence the improved removal of BB dyes obtained. Photocatalytic results could imply that both the aromatic rings and the azo groups of BB dyes are cleaved during photocatalytic reactions (Abidin *et al.,* 2015). *iii*) Further observation of the data available in Figure 6 from time 0 to 60 min under irradiation, it seems that the constant of the kinetic equation might not very identifiable, mainly in the case of 10% CNT–GOL. The first measurement at 15 min, already has all the concentration removed. It means that any rate higher that certain value would be also totally able to explain the experimental data. In addition, the increase in Ct/Ci for time 60 min cannot be explained by the commonly used models namely Langmuir-Hinshelwood (Kumar *et al.,* 2008; Asif *et al.,* 2015) and the pseudo-zero, pseudo-first

and second order kinetic models (Gaya., 2013). For future purpose, more experimental points would be needed before 15 min to have enough data to make the model easily identifiable. This is because 10% CNT–GOL demonstrated high efficiency within a short period of time than expected. The photocatalytic behaviour of 10% CNT–GOL nanocomposite would be better investigated with shorter time (i.e. every 5 min instead of 15 min) interval for taking aliquots. As such, we thought outside classical procedure to measure kinetics studies. The kinetic information obtained with these data is then carefully explained by only considering the first 45 min of the experiments. Data depicted in Figures 5 and 6 (a) obtained without the addition of H_2O_2 during the 45 min of the photocatalytic experiments were considered for the kinetic studies.

The Langmuir-Hinshelwood model was used, in the simplified form represented by equation (2), to describe the kinetics of photocatalytic reactions of small concentration in aqueous solutions:

$$\ln \frac{C_i}{C_f} = k_{app} t \qquad (2)$$

Where *Ci* is the initial concentration (ppm or mg L^{-1}) of BB dye after adsorption, *Ct* is the concentration (ppm or mg L^{-1}) of BB dye at time *t* during photocatalytic process. *Kapp* stands for the pseudo-first order reaction rate constant (min^{-1}), and *t* is irradiation time (min) during the photocatalytic reaction. The results are presented in Figure 7 for GOL clay, 5% CNT–GOL and 10% CNT–GOL photocatalysts. It is obvious from the linear fitting that the obtained data do not satisfactory obey the pseudo-first order kinetic model (Figure 7 (left hand side)).

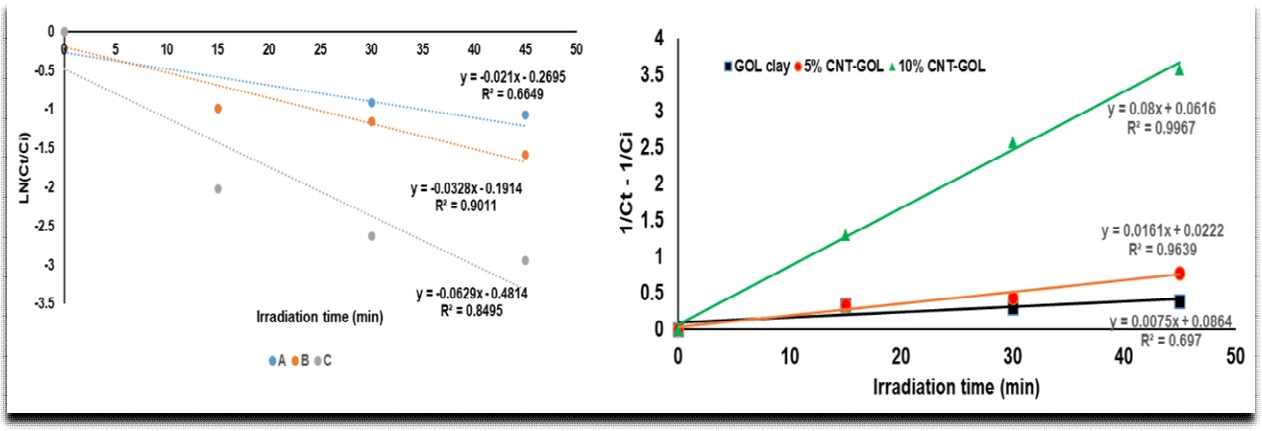


Figure 7. (Left hand side) Pseudo-first order kinetics of BB dyes degradation using GOL clay (A), 5% CNT–GOL (B) and 10% CNT–GOL (C) as photocatalysts under 45 min of visible light irradiation and (right hand side) second order model kinetics of BB dyes degradation using GOL clay, 5 % CNT–GOL and 10 % CNT–GOL as photocatalysts under 45 min of visible light irradiation.

Most dye-based oxidation studies rely on the disappearance of the initial concentration of dyes (Gaya, 2013). As such, the photocatalytic activity of the catalysts can be quantitatively evaluated by second order kinetic model in equation (3) where *Ci* and *Ct* are the initial concentration and concentration of BB dye at time (*t*) during the photocatalytic reaction, respectively.

$$-\frac{1}{[C_t]}+\frac{1}{[C_i]}=-kt \qquad (3)$$

A satisfactory fit was obtained for the photocatalysts that contain CNT (5% CNT–GOL and 10% CNT–GOL) in their composition as shown (Figure 7 (right hand side)) in agreement with previous reports (Kumar *et al.,* 2008; Wang *et al.,* 2015).

The photocatalytic experiments obtained in this study (at least for the points considered up to 45 min) show that the data fit well second order kinetic. This is important because it has been reported that an assumed reaction network leads to a single kinetic model, but a common model, the Langmuir–Hinshelwood rate equation, arises from multiple mechanisms, hence models alone

do not reveal unique mechanisms (Ollis, 2018). And the findings described herewith might worth sharing to inform researchers that certain photocatalytic experimental data might deviate from the classical procedure, alternative thinking might be necessary.

Proposed photocatalytic mechanism

The presence of CNT plays a role of semiconductor (Collins and Avouris, 2000) which emphasised the good quality of the 10% CNT–GOL sample to operate as a photocatalyst. The photodegradation of BB dyes was then improved by the ability of CNT to behave as an electron donor and acceptor. This is very crucial because, during photocatalysis, the excited e− in the conduction band of clay (SiO_2, Al_2O_3, TiO_2, Fe_2O_3) migrate into CNT, of which have a special structure and the ability for e− transport. Even interesting is that GOL clay acts as photoactive material and catalyst for the photodegradation (Martínez-Costa *et al.,* 2018). Thus, the possibility of the e^- / h^+ pairs recombination decreases. Meanwhile, the adsorbed oxygen (O_2) on the surface of CNTs may accept e^- and form radicals ($^{\bullet}O_2^-$), which also leads to the formation of other oxidizing species ($^{\bullet}OH$) in the system. Therefore, there are more radicals in the system, resulting in the quicker degradation of the BB dyes (Yu *et al.*, 2005; Saleh *and* Gupta, 2012). In this paper, the effect of H_2O_2 while varying the molar concentration to the aqueous solution of BB dyes during the photocatalytic experiments was assessed. H_2O_2 is one of the most used radical scavengers in photocatalysis (Muleja *and* Mamba, 2018). This is because H_2O_2 is a stronger electron acceptor than oxygen that can react with an electron emitted from the valence band of the photocatalyst to generate $^{\bullet}OH$ and OH^- (Chu *et al.,* 2007). Additionally, photoexcitation reaction of H_2O_2 produces $^{\bullet}OH$ species (Xu *et al.,* 2019) as displayed in equation (7) while equation (8) shows that more $^{\bullet}OH$ can be produced in the presence of $^{\bullet}O_2^-$. The results from H_2O_2 experiments confirm the important role of h^+ and $^{\bullet}OH$ during photocatalysis. The mixing of CNT and GOL clay could create an interface that can reduce the recombination of charge carrier pairs by the way of effective charge migration and separation, leading to the enhanced photocatalytic activity. Other researchers observed similar scenarios with different materials (Yin *et al.,* 2016; Luo *et al.,* 2019). The basic mechanism for the photodegradation of BB dyes with 10% CNT–GOL (CNT-Clay) is represented by the equations (4) to (11).

$$H_2O_2 \xrightarrow{h\nu} 2HO^{\bullet} \quad (4)$$

$$H_2O_2 + O_2^{\bullet -} \rightarrow HO^{\bullet} + O_2 + OH^- \quad (5)$$

$$CNT - Clay + h\nu \rightarrow CNT - Clay\left(e_{CB}^- + h\nu_{VB}^+\right) \quad (6)$$

$$CNT - Clay\left(h_{VB}^+\right) + H_2O \rightarrow CNT - Clay + HO^{\bullet} + H^+ \quad (7)$$

$$CNT - Clay\left(h_{VB}^+\right) + HO^- \rightarrow CNT - Clay + HO^{\bullet} \quad (8)$$

$$CNT - Clay\left(e_{CB}^-\right) + O_2 \rightarrow CNT - Clay + O_2^{\bullet -} \quad (9)$$

$$CNT - Clay\left(e_{CB}^-\right) + O_2^{\bullet -} \rightarrow CNT - Clay + H_2O_2 \quad (10)$$

$$BB + OH^- + O_2^{\bullet -} + h^+ \rightarrow CO_2 + H_2O + Organic\cdots compounds + Inorganic\cdots acids \quad (11)$$

Based on the above explanation, a mechanism of the mineralization of BB dyes under visible light irradiation is therefore suggested in a schematic representation in Figure 8.

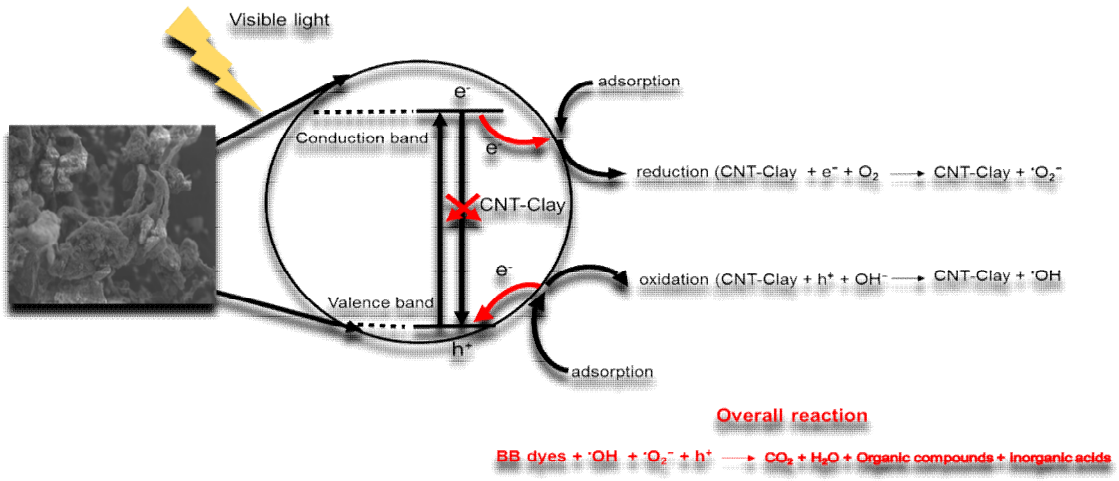


Figure 8. Proposed mechanism of photocatalytic degradation of BB dyes using 10 % CNT–GOL catalyst.

Total organic content analysis

Total organic content (TOC) analysis was used to investigate the amount of carbon element in organic compounds left in the aqueous solution after the photocatalytic experiments. This is important because it determines the level of BB dyes degradation during the photocatalysis with GOL clay, 5 % CNT–GOL and 10 % CNT–GOL materials. The TOC values of BB dye molecules removal were compared with the photodegradation removal percentage in order to estimate the level of mineralization of BB dyes. The results from the experiments carried out within 60 min are summarised in Table 2.

Table 2. Removal values for the degradation of BB dyes and TOC analysis of BB dyes in aqueous solution at time 60 min of solar light irradiation.

Percentage removal	**GOL clay**	**5 % CNT–GOL**	**10 % CNT–GOL**
TOC	35.97	39.95	86.14
Degradation	43.02	44.86	87.22

From Table 2, when GOL and 5 % CNT–GOL are used less than half (35.97 % and 39.95 %) of the amount of BB dyes molecules were removed. Yet with 10% CNT–GOL higher removal percentage (87.22 %) was obtained for the degradation of BB dyes. The data confirm that when 10 % CNT–GOL photocatalyst is used a higher degree of complete mineralisation of the dye molecules, which is desirable, was achieved. Higher TOC removal values indicate that the dye molecules are broken down into smaller colourless products first before being mineralized to carbon dioxide, water, and other inorganic species (Mamba *et al.* 2014). The results also show that a certain amount of organic degradation by-products remain in solution. The current mineralization percentage of BB dye molecules is higher (87 %) than previously reported 61 % (Nzaba *et al.,* 2018) and 62 % (Mukonza *et al.,* 2017) within an hour of visible light irradiation implying that GOL–CNT could be more suitable for the removal of BB dyes from aqueous solution.

Table 2 also reveals that when CNT was added to the natural clay, the percentage of BB dye molecules removal increased for both TOC and degradation from 35.97 % to 86.14 and 43.02 % to 87.22 % for GOL and 10 % CNT–GOL, respectively. The findings are interesting because they entail that CNT contributes significantly to the degradation of BB dyes in aqueous solution. There is a close correlation between the two values. However, when natural clay is used the level of TOC removal and that of degradation are 7.05 % apart indicating that some of the removal is due to the adsorption process which was expected because adsorption is desired for photocatalysis. The same observation is evident with 5 % CNT–GOL where 4.91 % less removal was obtained. On overall photocatalytic activity on BB dyes, a comparative survey shows that 10 % CNT–GOL performed better within an hour than PAMAM templated N,Pt co-doped TiO_2 (Nzaba *et al.*, 2018) and F, Sm^{3+} codoped TiO_2 (Mukonza *et al.*, 2017). Another advantage of the 10 % CNT–GOL photocatalyst is that at the end of experiments, the sedimentation and decantation of materials was easy and fast (Chen *et al.,* 2004) which would be essential for future study on recycling.

Conclusion

In this paper, natural clay and carbon nanotubes were mechanically mixed. The mixing produced natural nanocomposites with enhanced photocatalytic activity. Natural clay contains 2.34 % of TiO_2 which is crucial in photocatalysis and the DRS revealed that the materials can be used as photocatalysts. The addition of CNT to GOL reduced the energy band gaps from 3.25 eV (GOL) to 2.90 eV (10 % CNT–GOL) and 2.75 eV (GOL) to 1.53 eV (10 % CNT–GOL) for the first and second absorption bands, respectively. CNT contributed to the enhancement of the photocatalytic activity of CNT–GOL nanocomposites through the charges migration, separation and reduction of the recombination of the e^- / h^+ pairs. Furthermore, the mixing of CNT and GOL created a synergy and formation of a heterojunction like interface improving the photocatalytic features of the nanocomposites. All these aspects added to the production of highly oxidizing radical species which attacked the azo and amines groups in BB dyes leading to their degradation. The kinetic data (based on 45 min time of light irradiation) showed that the photocatalysis decay of BB dyes fit well the second order model. The TOC results showed that 87 % of the BB dye molecules were completely mineralized in 60 min when 10 % CNT–GOL was used. The 10% CNT–GOL successfully removed 95 % BB dyes while 66 % removal was obtained for the GOL. The performance was further increased with the addition of 2 mmoL of H_2O_2 within 15 min of solar light irradiation. The current study showed that when optimized natural clay mixed with CNT could find application as a modified photocatalytic filter for the treatment of wastewaters in the rural areas where clays and sun light are readily available.

Acknowledgements

This work was financially supported by the University of South Africa (UNISA) at the Institute for Nanotechnology and Water Sustainability (iNanoWS), College of Science, Engineering and Technology (CSET).

References

Abidin, C. Z. A., Fahmi, M. R., Soon-An, O., Makhtar, S. N. N. M. and Rahmat, N. R. (2015) Decolourization of an azo dye in aqueous solution by ozonation in a semi-batch bubble column reactor. *Science Asia,* **41**, 49-54.

Al-Kdasi, A., Idris, A., Saed, K. and Guan, C.T. (2004) Treatment of textile wastewater by advanced oxidation processes—a review. *Global nest: the Int. J,* **6**(3), 222-230.

Asif, S. A. B., Khan, S. B. and Asiri, A. M. (2015) Visible light functioning photocatalyst based on Al2O3 doped Mn3O4 nanomaterial for the degradation of organic toxin. *Nanoscale research letters*, **10**(1), 355.

Boukhemkhem, A. and Rida, K. (2017) Improvement adsorption capacity of methylene blue onto modified Tamazert kaolin. *Adsorption Science & Technology*, **35**(9-10), 753-773.

Brüschweiler, B.J. and Merlot, C. (2017) Azo dyes in clothing textiles can be cleaved into a series of mutagenic aromatic amines which are not regulated yet. *Regulatory Toxicology and Pharmacology*, **88**, 214-226.

Chargui, F., Hamidouche, M., Belhouchet, H., Jorand, Y., Doufnoune, R. and Fantozzi, G. (2018) Mullite fabrication from natural kaolin and aluminium slag. *Boletín de la Sociedad Española de Cerámica y Vidrio*, **57**(4), 169-177.

Chen, Y., Wang, K. and Lou, L. (2004) Photodegradation of dye pollutants on silica gel supported TiO2 particles under visible light irradiation. *Journal of Photochemistry and Photobiology A: Chemistry*, **163**(1-2), 281-287.

Cheng, X., Zhong, J., Meng, J., Yang, M., Jia, F., Xu, Z., Kong, H. and Xu, H. (2011) Characterization of multiwalled carbon nanotubes dispersing in water and association with biological effects. *Journal of Nanomaterials*, **2011**, 14.

Chu, W., Choy, W. K. and So, T. Y. (2007) The effect of solution pH and peroxide in the TiO2-induced photocatalysis of chlorinated aniline. *Journal of hazardous materials*, **141**(1), 86-91.

Collins, P. G. and Avouris, P. (2000) Nanotubes for electronics. *Scientific American*, **283**(6), 62–69.

da Silva Lopes, J., Rodrigues, W. V., Oliveira, V. V., Braga, A. D. N. S., da Silva, R. T., França, A. A. C., da Paz, E. C., Osajima, J. A. and da Silva Filho, E. C. (2019) Modification of kaolinite from Pará/Brazil region applied in the anionic dye photocatalytic discoloration. *Applied Clay Science*, **168**, 295-303.

Djouadi, L., Khalaf, H., Boukhatem, H., Boutoumi, H., Kezzime, A., Santaballa, J. A. and Canle, M. (2018) Degradation of aqueous ketoprofen by heterogeneous photocatalysis using Bi2S3/TiO2–Montmorillonite nanocomposites under simulated solar irradiation. *Applied Clay Science*, **166**, 27-37.

Ebbesen, T. W., Lezec, H. J., Hiura, H., Bennett, J. W., Ghaemi, H. F. and Thio, T. (1996) Electrical conductivity of individual carbon nanotubes. Nature. **382**, 54-56.

Gaya, U.I. 2013 Heterogeneous photocatalysis using inorganic semiconductor solids. Springer Science and Business Media

Gournis, D., Karakassides, M. A., Bakas, T., Boukos, N., and Petridis, D. (2002). Catalytic synthesis of carbon nanotubes on clay minerals. Carbon, **40**(14), 2641-2646.Guldi, D. M., Rahman, G. M. A., Zerbetto, F. and Prato, M. (2005) Carbon nanotubes in electron donor−acceptor nanocomposites. *Accounts of Chemical Research*, **38**(11), 871-878.

Guo, J. 2007 Electronic structure characterization and bandgap engineering of solar hydrogen materials. In Solar Hydrogen and Nanotechnology II (Vol. 6650, p. 66500F). International Society for Optics and Photonics.

Hadjltaief, H. B., Gálvez, M. E., Zina, M. B., and Da Costa, P. (2019). TiO2/clay as a heterogeneous catalyst in photocatalytic/photochemical oxidation of anionic reactive blue 19. Arabian Journal of Chemistry, 12(7), 1454-1462.

Hamza, W., Dammak, N., Hadjltaief, H. B., Eloussaief, M. and Benzina, M. (2018) Sono-assisted adsorption of cristal violet dye onto tunisian smectite clay: Characterization, kinetics and adsorption isotherms. *Ecotoxicology and environmental safety*, **163**, 365-371.

Herrmann, J. M. 1999 Heterogeneous photocatalysis: fundamentals and applications to the removal of various types of aqueous pollutants. *Catalysis today*, **53**(1), 115-129.

Horwath, W., and Liang, Y. L. (2011). Variations of Chemical Composition and Band Gap Energies in Hectorite and Montmorillonite Clay Minerals on Sub-Micron Length Scales. Final Report. Kearney Foundation of Soil Science.

Kausar, A., Iqbal, M., Javed, A., Aftab, K., Bhatti, H.N. and Nouren, S. (2018) Dyes adsorption using clay and modified clay: A review. *Journal of Molecular Liquids*, **256**, 395-407

Khennaoui, B., Zehani, F., Malouki, M. A., Menacer, R., and López, M. C. (2020). Chemical and physical characterization of a natural clay and its use as photocatalyst for the degradation of the methabenzthiazuron herbicide in water. Optik, 219, 165024.

Kumar, K. V., Porkodi, K. and Rocha, F. (2008) Langmuir–Hinshelwood kinetics–a theoretical study. *Catalysis Communications*, **9**(1), 82-84.

Leow, W. R., Ng, W. K. H., Peng, T., Liu, X., Li, B., Shi, W., Lum, Y., Wang, X., Lang, X., Li, S. and Mathews, N. (2016) Al2O3 surface complexation for photocatalytic organic transformations. *Journal of the American Chemical Society*, **139**(1), 269-276.

Li, J. and Bishop, P. L. (2002) In situ identification of azo dye inhibition effects on nitrifying biofilms using microelectrodes. *Water science and technology*, **46**(1-2), 207-214.

Luo, J., Luo, Y., Yao, J., Zhang, M., Chen, S. and Liu, X. (2019) Composite microsphere resulting from assembly of BiOCl nanosheets and palygorskite nanorods for enhanced photocatalytic activity. *Applied Clay Science*, **168**, 450-458.

Mamba, G., Mamo, M. A., Mbianda, X. Y. and Mishra, A. K. (2014) Nd, N, S-TiO_2 decorated on reduced graphene oxide for a visible light active photocatalyst for dye degradation: Comparison to its MWCNT/Nd, N, S-TiO_2 analogue. *Industrial & Engineering Chemistry Research*, **53**(37), 14329-14338.

Martínez-Costa, J.I., Rivera-Utrilla, J., Leyva-Ramos, R., Sánchez-Polo, M. and Velo-Gala, I. (2018) Individual and simultaneous degradation of antibiotics sulfamethoxazole and trimethoprim by UV and solar radiation in aqueous solution using bentonite and vermiculite as photocatalysts. *Applied Clay Science*, **160**, 217-225.

Masheane, M., Nthunya, L., Mubiayi, M., Thamae, T. and Mhlanga, S. (2018) Physico-chemical characteristics of some Lesotho's clays and their assessment for suitability in ceramics production. *Particulate Science and Technology*, **36**(1), 117-122.

Matsumoto, Y. 1996 Energy positions of oxide semiconductors and photocatalysis with iron complex oxides. *Journal of solid state chemistry*, **126**(2), 227-234.

Molinari, R., Lavorato, C. and Argurio, P. (2017) Recent progress of photocatalytic membrane reactors in water treatment and in synthesis of organic compounds. A review. *Catalysis Today*, **281**, 144-164.

Mukonza, S. S., Nxumalo, E. N., Mamba, B. B. and Mishra, A. K. (2017) Enhanced solar light photodegradation of brilliant black bisazo dye in aqueous solution by F,Sm^{3+} codoped TiO2. *IOP Conference Series: Materials Science and Engineering* (Vol. 195, No. 1, p. 012006). IOP Publishing.

Muleja, A. A. and Mamba, B. B. (2018) Development of calcined catalytic membrane for potential photodegradation of Congo red in aqueous solution. *Journal of environmental chemical engineering*, **6**(4), 4850-4863.

Muleja, A. A., Mbianda, X. Y., Krause, R. W., and Pillay, K. (2012). Synthesis, characterization and thermal decomposition behaviour of triphenylphosphine-linked multiwalled carbon nanotubes. Carbon, **50**(8), 2741-2751.

Nazarkovsky, M. A., Gun'ko, V.M., Wójcik, G., Czech, B., Sobieszek, A., Skubiszewska-Zięba, J., Janusz, W. and Skwarek, E. (2014) Band-gap change and photocatalytic activity of silica/titania composites associated with incorporation of CuO and NiO. *Chemistry, Physics and Technology of Surface.* **5**, 421-437.

Nzaba, S. K. M., Ntsendwana, B., Mamba, B. B. and Kuvarega, A. T. (2018) PAMAM templated N, Pt co-doped TiO2 for visible light photodegradation of brilliant black. *Environmental Science and Pollution Research*, **25**(15), 15146-15158.

Oh, S. W., Kang, M. N., Cho, C. W. and Lee, M. W. (1997) Detection of carcinogenic amines from dyestuffs or dyed substrates. *Dyes and Pigments*, **33**(2), 119-135.

Oh, W. C., Zhang, F. J. and Chen, M. L. (2010) Characterization and photodegradation characteristics of organic dye for Pt–titania combined multi-walled carbon nanotube composite catalysts. *Journal of industrial and engineering chemistry*, **16**(2), 321-326.

Ollis, D. F. 2018 Kinetics of Photocatalyzed Reactions: five lessons learned. *Frontiers in chemistry*, **6.**

Paredes, S. P., Valenzuela, M. A., Fetter, G., and Flores, S. O. (2011). TiO_2/MgAl layered double hydroxides mechanical mixtures as efficient photocatalysts in phenol degradation. *Journal of physics and Chemistry of solids*, 72(8), 914-919.

Rafii, F., Hall, J. D. and Cerniglia, C. E. (1997) Mutagenicity of azo dyes used in foods, drugs and cosmetics before and after reduction by Clostridium species from the human intestinal tract. *Food and chemical Toxicology*, **35**(9), 897-901.

Saleh, T. A. and Gupta, V. K. (2012) Photo-catalyzed degradation of hazardous dye methyl orange by use of a composite catalyst consisting of multi-walled carbon nanotubes and titanium dioxide. *Journal of Colloid and Interface Science*, **371**(1), 101-106.

Terzopoulou, Z., Bikiaris, D.N., Triantafyllidis, K.S., Potsi, G., Gournis, D., Papageorgiou, G.Z. and Rudolf, P. (2016) Mechanical, thermal and decomposition behavior of poly (ε-caprolactone) nanocomposites with clay-supported carbon nanotube hybrids. *Thermochimica Acta*, **642**, 67-80.

Todorova, N., Giannakopoulou, T., Karapati, S., Petridis, D., Vaimakis, T. and Trapalis, C. (2014) Composite TiO_2/clays materials for photocatalytic NOx oxidation. *Applied Surface Science*, **319**, 113-120.

Wang, Y., Zhou, A., Jiang, Y., Chen, X. and He, J. (2015) Tetraamino-zinc phthalocyanine covalently bound to benzoic acid-functionalized graphene composites for highly efficient visible light photocatalytic activities. *RSC Advances*, **5**(47), 37823-37829.

Wei, H., Gu, H., Guo, J., Wei, S. and Guo, Z. (2013) Multiwalled carbon nanotubes with tuned surface functionalities for electrochemical energy storage. *ECS Journal of Solid State Science and Technology*, **2**(10), M3008-M3014.

Xu, M., Pan, G., Meng, Y., Guo, Y., Wu, T. and Chen, H. (2019) Effect of Ce3+ on the photocatalytic activity of MAlCe ternary hydrotalcites-like compounds in methylene blue photodegradation. *Applied Clay Science*, **170**, 46-56.

Yamaguchi, K., Inumaru, K., Oumi, Y., Sano, T., and Yamanaka, S. (2009). Photocatalytic decomposition of 2-propanol in air by mechanical mixtures of TiO2 crystalline particles and silicalite adsorbent: The complete conversion of organic molecules strongly adsorbed within zeolitic channels. Microporous and mesoporous materials, 117(1-2), 350-355.

Yin, S., Di, J., Li, M., Fan, W., Xia, J., Xu, H., Sun, Y. and Li, H. (2016) Synthesis of Multiwalled Carbon Nanotube Modified BiOCl Microspheres with Enhanced Visible-Light Response Photoactivity. *CLEAN–Soil, Air, Water*, **44**(7), 781-787.

Yu, Y., Jimmy, C. Y., Chan, C. Y., Che, Y. K., Zhao, J. C., Ding, L., Ge, W. K. and Wong, P. K. (2005) Enhancement of adsorption and photocatalytic activity of TiO2 by using carbon nanotubes for the treatment of azo dye. *Applied Catalysis B: Environmental*, **61**(1-2), 1-11.

Zeitler, V. A. and Brown, C. A. (1957) The Infrared Spectra of Some Ti-O-Si, Ti-O-Ti and Si-O-Si Compounds. *The Journal of Physical Chemistry*, **61**(9), 1174-1177.

Zhu, W., Miser, D. E., Chan, W. G. and Hajaligol, M. R. (2004) Characterization of combustion fullerene soot, C60, and mixed fullerene. *Carbon*, **42**(8-9), 1463-1471.



https://dspace.org/

Titania containing natural clay doped with carbon nanotubes for enhanced natural photocatalytic discoloration of wastewater

Muleja, A. A.; Mubiayi, M. P.; Hassard, Francis; Mamba, B. B.

2021-04-17
Springer
https://doi.org/10.1007/s11051-021-05194-5
Muleja AA, Mubiayi MP, Hassard F, Mamba BB. (2021) Titania containing natural clay doped with carbon nanotubes for enhanced natural photocatalytic discoloration of wastewater. Journal of Nanoparticle Research, Volume 23, April 2021, Article number 97

Downloaded from a DSpace repository. https://dspace.org/